

# Metamaterial band theory: fundamentals & applications

RAMAN Aaswath Pattabhi, SHIN Wonseok & FAN ShanHui\*

*Ginzton Laboratory, Stanford University Stanford, CA 94305, USA*

Received August 12, 2013; accepted October 31, 2013

**Abstract** Remarkable progress has been made over the past decade in controlling light propagation and absorption in compact devices using nanophotonic structures and metamaterials. From sensing and modulation, to on-chip communication and light trapping for solar cells, new device applications and opportunities motivate the need for a rigorous understanding of the modal properties of metamaterials over a broad range of frequencies. In this review, we provide an overview of a metamaterial band theory we have developed that rigorously models the behavior of metamaterials made of dispersive materials such as metals. The theory extends traditional photonic band theory for periodic dielectric structures by coupling the mechanical motion of electrons in the metal directly to Maxwell's equations. The solution for the band structures of metamaterials is then reduced to a standard matrix eigenvalue problem that nevertheless fully takes into account the dispersive properties of the constituent materials. As an application of the metamaterial band theory, we show that one can develop a perturbation formalism based on this theory to physically explain and predict the effect of dielectric refractive index modulation or metallic plasma frequency variation in metamaterials. Furthermore, the metamaterial band theory also provides an intuitive physical picture of the source of modal material loss, as well as a rigorous upper bound on the modal material loss rate of any plasmonic, metamaterial structure. This in turn places fundamental limits on the broadband operation of such devices for applications such as photodetection and absorption.

**Keywords** metamaterials, photonic band theory, plasmonics, sensing, active metamaterials

**Citation** Raman A P, Shin W, Fan S H. Metamaterial band theory: fundamentals & applications. *Sci China Inf Sci*, 2013, 56: 120402(14), doi: 10.1007/s11432-013-5039-7

## 1 Introduction

The past two decades have seen extraordinary advances in the study and understanding of nanoscale photonic structures such as photonic crystals and metamaterials. As researchers have sought to fully characterize and explore the physical phenomena possessed by such nanophotonic structures, it has become increasingly necessary to understand how such structures behave over a broad range of frequencies. Harkening back to early studies of the broadband response of natural materials to light, it is both of intrinsic and applied interest to develop an analytical, physical framework capable of describing the electromagnetic modes of all metamaterial systems in a general way: a metamaterial band theory.

\*Corresponding author (email: shanhui@stanford.edu)

While metamaterials often lend themselves to an effective-index picture [1], many metamaterial designs, including fishnets [2] and chiral structures [3], have feature sizes that necessitate band structure computations to understand their behavior. The need to accurately calculate the eigenmodes and band structures of such periodic structures numerically, and place analytic constraints on the modes of metamaterial systems whose constituent materials are typically dispersive and metallic, motivates the development of a rigorous metamaterial band theory.

The photonic band structure for any periodic material system can, in general, be determined by solving the following equation [4]:

$$\nabla \times \frac{1}{\varepsilon} \nabla \times \mathbf{H} = \left(\frac{\omega}{c}\right)^2 \mathbf{H}, \quad (1)$$

where  $\varepsilon$  is the material permittivity,  $\mathbf{H}$  is the magnetic field and  $\omega$  is the frequency of the photonic mode. When  $\varepsilon$  is lossless and frequency-independent, Eq. (1) becomes a Hermitian eigenvalue problem [4]. Such a Hermitian formalism greatly facilitates numerical calculations [5]. In addition, it ensures mode-orthogonality across different bands, which permits a global view of the band structure [4], and enables advanced simulation techniques such as the Wannier function approach that speed up the calculation of complex photonic circuits [6,7].

Since metamaterials are composed of dispersive materials, there is great interest in performing similar band structure calculations for material systems with arbitrary frequency-dependent dielectric functions,  $\varepsilon(\omega)$ . The challenge here is that with the  $\omega$  dependence in  $\varepsilon$ , Eq. (1) no longer defines a standard eigenvalue problem. While the photonic band structures for such dispersive systems have been obtained by a variety of techniques that solve Maxwell's equations in either the time or frequency domains [8–16], in all these formalisms there are no apparent constraints between solutions at different bands. The resulting band structures are thus of less utility than the standard dielectric band structure, since many important calculations, such as the calculations of local density of states [17], rely critically on the ability to expand the fields on an orthonormal basis formed by the eigenmodes of the system.

Beyond band structure computation, the development of a metamaterial band theory would also allow one to fully study and characterize important metamaterial device applications. In particular, there has been substantial recent interest in using metamaterials for active devices and sensing. While surface-plasmon sensors are already prominent in biochemical sensing applications [18,19], remarkable improvements in device performance have been achieved using plasmonic nanostructures and metamaterial approaches [20–22]. Active plasmonic devices have also been implemented for modulation and switching [23–27].

The development of metamaterial device applications is ultimately contingent on basic physical limits related to the use of dispersive materials such as metals in these systems. The coupling of photons to the electrons in the metal enables deep subwavelength modal confinement, but also results in a powerful absorption and loss mechanism for electromagnetic modes in such metallic systems. This optical loss is a limiting factor for some applications [28–35]. On the other hand, enhanced optical loss in plasmonic systems has recently been leveraged to improve and maximize absorption for a range of applications [36] including ultra-thin absorbers [37] and photodetectors [38]. The fundamental framework offered by a metamaterial band theory could, in turn, place constraints on the universal behavior of metamaterial modes as they relate to loss.

In this paper, we review a rigorous metamaterial band theory developed by the authors in three previous works [39–41]. This review article is organized as follows. In Section 2, we demonstrate that the band structure of dispersive photonic crystals and optical metamaterials, in general, can be obtained by solving a standard matrix eigenvalue problem. In the case where the material can be approximated as lossless, the eigenvalue problem is Hermitian, which directly leads to an orthogonality-condition for modes at different frequencies. In Section 3, this metamaterial band theory is numerically implemented using a finite-difference scheme. 2D periodic arrays of plasmonic rods in air are studied using the numerical implementation where the plasmonic material is defined by a two-pole fit of silver's dielectric function. In Section 4 we build upon the band theory to construct a metamaterial perturbation theory that can generally treat the effect of small changes in any system parameter, whether geometric or material. In

Section 5 we use the perturbation theory to predict modal frequency shifts due to changes in the dielectric constants of dispersive systems involving both metals and dielectrics. In Section 6, we prove rigorously that, for any electromagnetic mode of a plasmonic metamaterial structure, there exists an upper bound on its material loss rate. When the plasmonic material is described by a multi-pole Lorentz model, the upper bound is a frequency-dependent weighted-average of the damping rates of the oscillators that underlie the poles. We validate this proof by full-field simulations of a variety of systems including periodic arrays of slot antennas [41]. Finally, we conclude in Section 7 and consider other recent uses of the band theory.

## 2 Metamaterial band theory formulation

We begin our analysis by considering materials whose permittivities can be described by

$$\varepsilon(\omega) = \varepsilon_\infty + \varepsilon_\infty \sum_{n=1}^N \frac{\omega_{p,n}^2}{\omega_{0,n}^2 - \omega^2 + i\omega\Gamma_n}. \quad (2)$$

This is the standard  $N$ -pole Lorentz-Drude function used to fit the permittivities of dispersive materials such as metals or polaritonic materials. As a short-hand we refer to all such materials as metals in the rest of the paper but emphasize that the results reviewed herein extend to any material system whose dielectric function can be described by a fit to Lorentz poles. The  $n$ th pole is characterized by its resonant frequency  $\omega_{0,n}$ , its damping rate  $\Gamma_n$ , and its oscillator strength  $\omega_{p,n}$ . For many metals in the optical wavelength range, such as silver [42], it is essential to use multiple poles in order to capture contributions to the permittivities from both intra-band, and inter-band transitions. The intra-band transition gives rise to free-electron behavior that is characterized by a Drude pole with its resonant frequency  $\omega_0 = 0$ , whereas the inter-band transition gives rise to a Lorentz pole.

To describe such a dispersive material, for the  $n$ th pole in the dielectric function, one introduces a polarization field  $\mathbf{P}_n$  and a polarization velocity field  $\mathbf{V}_n$ , satisfying

$$\frac{\partial \mathbf{P}_n}{\partial t} = \mathbf{V}_n, \quad (3)$$

$$\frac{\partial \mathbf{V}_n}{\partial t} = \omega_{p,n}^2 \varepsilon_\infty \mathbf{E} - \omega_{0,n}^2 \mathbf{P}_n - \Gamma_n \mathbf{V}_n. \quad (4)$$

These auxiliary fields [43,44] are then coupled to Maxwell's equations through

$$\frac{\partial \mathbf{H}}{\partial t} = -\frac{1}{\mu_0} \nabla \times \mathbf{E}, \quad (5)$$

$$\frac{\partial \mathbf{E}}{\partial t} = \frac{1}{\varepsilon_\infty} \left( \nabla \times \mathbf{H} - \sum_{n=1}^N \mathbf{V}_n \right). \quad (6)$$

For steady state, with fields varying as  $\exp(i\omega t)$ , Eqs. (3)–(6) become

$$i\omega \mathbf{H} = -\frac{1}{\mu_0} \nabla \times \mathbf{E}, \quad (7)$$

$$i\omega \mathbf{E} = \frac{1}{\varepsilon_\infty} (\nabla \times \mathbf{H} - \sum_{n=1}^N \mathbf{V}_n), \quad (8)$$

$$i\omega \mathbf{P}_n = \mathbf{V}_n, \quad (9)$$

$$i\omega \mathbf{V}_n = \omega_{p,n}^2 \varepsilon_\infty \mathbf{E} - \omega_{0,n}^2 \mathbf{P}_n - \Gamma_n \mathbf{V}_n, \quad (10)$$

and thus define an eigenvalue problem for  $\omega$ . Closely related to this approach, we note that similar auxiliary fields have been employed in standard finite-difference time-domain simulations for dispersive media [44], and have been used as a starting point for field quantization in dispersive media [45]. Eqs. (7)–(10) also define a total energy density

$$W_0 = \frac{1}{4} (\varepsilon_\infty |\mathbf{E}|^2 + \mu_0 |\mathbf{H}|^2) + \sum_{n=1}^N \frac{1}{4\varepsilon_\infty \omega_{p,n}^2} (\omega_{0,n}^2 |\mathbf{P}_n|^2 + |\mathbf{V}_n|^2). \quad (11)$$

The spatial integral of (11), which represents the total energy of the system, is conserved when  $\Gamma_n = 0$  for all poles. Further, defining  $\mathbf{x} = (\mathbf{H}, \mathbf{E}, \mathbf{P}_1, \mathbf{V}_1, \dots, \mathbf{P}_N, \mathbf{V}_N)^\top$ , which represents a multi-component vector field varying over the whole space, we can write (7)–(10) as [39]

$$\omega \mathbf{A} \mathbf{x} = \mathbf{B} \mathbf{x}, \quad (12)$$

where  $\mathbf{A} = \text{diag}(\mu_0, \varepsilon_\infty, \dots, \omega_{0,N}^2/\omega_{p,N}^2 \varepsilon_\infty, 1/\omega_{p,N}^2 \varepsilon_\infty)$  and

$$\mathbf{B} = \begin{pmatrix} 0 & i\nabla \times \dots & 0 & 0 \\ -i\nabla \times & 0 & \dots & 0 \\ \vdots & \ddots & & \vdots \\ 0 & 0 & \dots & 0 \\ 0 & -i & \dots & i \end{pmatrix}. \quad (13)$$

Finally, defining  $\mathbf{y} = \sqrt{\mathbf{A}} \mathbf{x}$ , we can re-write this as an eigenvalue equation for  $\omega$ :

$$\omega \mathbf{y} = (\sqrt{\mathbf{A}})^{-1} \mathbf{B} (\sqrt{\mathbf{A}})^{-1} \mathbf{y}. \quad (14)$$

For the lossless case,  $\Gamma_n = 0$ , Eq. (14) becomes a Hermitian eigenvalue equation which results in an orthonormality condition closely connected to the energy density expression previously introduced:

$$\int d\mathbf{r} \left[ \frac{1}{4} (\varepsilon_\infty \mathbf{E}_a^* \cdot \mathbf{E}_b + \mu_0 \mathbf{H}_a^* \cdot \mathbf{H}_b) + \sum_{n=1}^N \frac{1}{4\varepsilon_\infty \omega_{p,n}^2} (\omega_{0,n}^2 \mathbf{P}_{a,n}^* \cdot \mathbf{P}_{b,n} + \mathbf{V}_{a,n}^* \cdot \mathbf{V}_{b,n}) \right] = \delta_{ab}. \quad (15)$$

### 3 Numerical band structure calculation

To numerically compute the band structure, we implement a finite-difference spatial discretization of the  $\mathbf{E}$  and  $\mathbf{H}$  fields with a Yee grid [46]. The use of Yee's grid ensures divergence-free behavior for the electromagnetic fields [43]. The equations are written for every cell in the Yee grid, with the spatial derivatives represented using finite-difference matrix operators [47]. Below, we will only examine systems with 2D periodicity for simplicity, but we note here that our method is not constrained to 2D, and can be used for 3D periodic systems. The Hermitian eigenvalue problem of (14) in particular can be solved efficiently using the well-known Implicitly Restarted Lanczos Method [48]. The formalism introduced has also been implemented in 3D using finite-element approaches [3].

As a specific example, we consider as our model system a 2D periodic array of square plasmonic rods in air where the plasmonic material is described by a Lorentz-pole fit of silver's permittivity. The system has periodicity  $a = 130$  nm and the rod has a side length of  $s = 0.45a = 58.5$  nm.

The plasmonic metal's dielectric function is defined by fitting silver's tabulated permittivity [49] with a Lorentz-Drude model [42], consisting of a Lorentz pole and a Drude pole. In Figure 1(a) we see that using the two poles is more accurate than using the Drude model alone for modeling silver's dielectric function at optical frequencies. The Lorentz pole in this fit is defined by  $\omega_{0,1} = 0.5526$ ,  $\omega_{p,1} = 0.8196$ , and  $\Gamma_1 = 0.1195$ , and the Drude pole by  $\omega_{0,2} = 0$ ,  $\omega_{p,2} = 0.9615$ , and  $\Gamma_2 = 0.0022$ . All frequencies in the numerical examples are normalized to  $2\pi c/a$ . A plot of the real and imaginary parts of this fit over the relevant normalized frequency range is presented in Figure 1(b). In the formalism of Section 2, the Drude pole has zero resonant frequency, and hence only requires the  $\mathbf{V}$ -field as its auxiliary field. Thus, in our system, we describe the effects of dispersion in terms of three auxiliary fields:  $\mathbf{P}_1$  and  $\mathbf{V}_1$  for the Lorentz pole, and  $\mathbf{V}_2$  for the Drude pole.

We analyze the TM and TE modes (with their electric and magnetic fields respectively polarized along the  $z$ -dimension) of this system in Figure 2. In our finite difference implementation, we have truncated the finite-difference grid appropriately at the metal-air interface to ensure that boundary conditions for

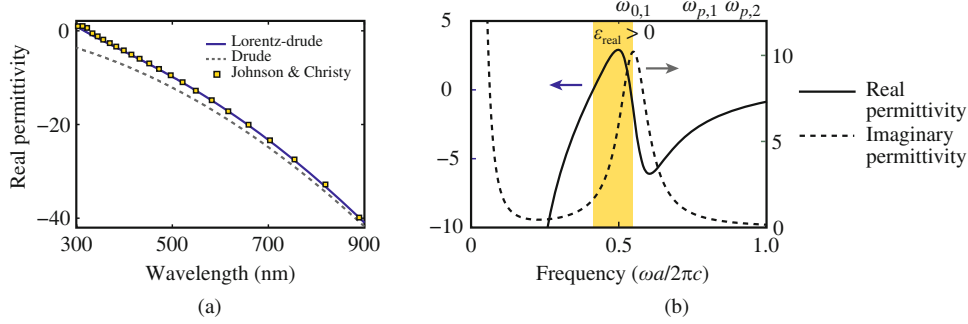


**Figure 1** (a) Comparing tabulated data for the real part of silver's permittivity [49] against the Drude model and Lorentz-Drude [42] fit used in this paper, at optical wavelengths; (b) the imaginary and real parts of the Lorentz-Drude fit [42] of silver's permittivity over normalized frequencies for  $a = 130$  nm.

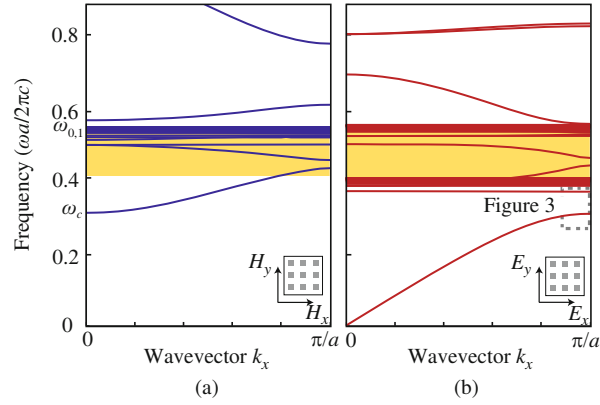


**Figure 2** Computed band structures for a square lattice of 2D plasmonic rods ( $s = 0.45a$ ) in air for the (a) TM and (b) TE polarization between ( $k_x = 0, k_y = 0$ ) and ( $k_x = \pi/a, k_y = 0$ ) points. The metal is describe by a Lorentz-Drude fit of silver with the presence of the Lorentz pole at  $\omega_{0,1}$  highlighted. The cutoff frequency for TM modes is identified at  $\omega_c$ , and frequency regions where  $\text{Re}[\epsilon] > 0$  are highlighted in yellow.

the tangential field components of the  $E$ -field are satisfied at these interfaces [50]. For the TM case, we find that a stop-band exists below a cutoff frequency  $\omega_c = 0.3067$ . In the TE case we note the presence of dispersion-less flat bands below  $\omega \approx 0.4$  that correspond to surface plasmon modes, and modes that have substantial group velocity which correspond to non-surface modes. For both cases, we also observe the presence of a dense cluster of low group-velocity modes right below  $\omega_{0,1}$  [51] in the region where  $\text{Re}[\epsilon] > 0$ , highlighted yellow in Figure 1(b) and Figure 2.

## 4 Metamaterial perturbation theory

We now review a general perturbation theory [40] based on the generalized eigenvalue equation for the photonic bands of dispersive nanostructures (12) developed in Section 2. We start from the unperturbed system

$$\omega_0 \mathbf{A}_0 \mathbf{x}_0 = \mathbf{B}_0 \mathbf{x}_0. \quad (16)$$

In the presence of a perturbation, the system matrices become  $\mathbf{A} = \mathbf{A}_0 + \mathbf{A}_1$ , and  $\mathbf{B} = \mathbf{B}_0 + \mathbf{B}_1$ , and as a result, we have

$$(\omega_0 + \omega_1)(\mathbf{A}_0 + \mathbf{A}_1)(\mathbf{x}_0 + \mathbf{x}_1) = (\mathbf{B}_0 + \mathbf{B}_1)(\mathbf{x}_0 + \mathbf{x}_1). \quad (17)$$

Using (16) and keeping only first-order terms in (17), we have

$$\omega_0 \mathbf{A}_0 \mathbf{x}_1 + \omega_1 \mathbf{A}_0 \mathbf{x}_0 + \omega_0 \mathbf{A}_1 \mathbf{x}_0 = \mathbf{B}_0 \mathbf{x}_1 + \mathbf{B}_1 \mathbf{x}_0. \quad (18)$$

Eq. (16), in its most general form, describes a lossy system and cannot be written as a Hermitian eigenvalue problem. Thus, to calculate  $\omega_1$  we also need to determine the left eigenvector  $\mathbf{z}_0$  that satisfies

$$\omega_0 \mathbf{z}_0 \mathbf{A}_0 = \mathbf{z}_0 \mathbf{B}_0. \quad (19)$$

Multiplying  $\mathbf{z}_0$  through (18) and solving for  $\omega_1$ , we find

$$\omega_1 = \frac{\mathbf{z}_0 \mathbf{B}_1 \mathbf{x}_0 - \omega_0 \mathbf{z}_0 \mathbf{A}_1 \mathbf{x}_0}{\mathbf{z}_0 \mathbf{A}_0 \mathbf{x}_0}. \quad (20)$$

In Section 5, we apply this equation to an example of a perturbation in metamaterial systems: dielectric refractive-index modulation.

## 5 Dielectric refractive-index modulation

To design active optical devices such as sensors, switches and modulators, one must calculate how a small change in refractive index affects the device's response function. For active devices based on dielectric structures [52–56] described by a frequency-independent dielectric constant distribution  $\varepsilon(\mathbf{r})$ , the effect of an index change is described by a frequency shift  $\omega_1$  of the eigenmodes of the system, which is given by first-order perturbation theory as [53,57]

$$\omega_1 = -\frac{\omega \int d\mathbf{r} \Delta\varepsilon(\mathbf{r}) |\mathbf{E}(\mathbf{r})|^2}{2 \int d\mathbf{r} \varepsilon(\mathbf{r}) |\mathbf{E}(\mathbf{r})|^2}. \quad (21)$$

The numerator in (21) only has contributions from the perturbed regions as described by  $\Delta\varepsilon(\mathbf{r})$ . The shift in the eigenfrequency thus depends on the overlap of the modal electric field energy with the perturbed region.

Eq. (21), however, is not applicable for metamaterial systems.  $\varepsilon(\mathbf{r})$  can be negative in a metal system, and thus directly applying (21) could lead to an unphysical prediction of infinite sensitivity. Moreover, in plasmonic systems, recent experiments have successfully varied the plasma frequency of the metal [58–60], introducing a new degree of freedom that requires formal theoretical treatment. While we do not review the specific case of plasma frequency variation in this paper, we showed in our original work [40], that this case can be effectively treated using the perturbation formalism.

In this section we focus on the specific case of a small change ( $\Delta\varepsilon(\mathbf{r})$ ) in the dielectric constant of a dielectric region, in a nanostructure consisting of both metal and dielectric regions. The metal region is assumed to be unperturbed. In this case, the perturbation takes the form

$$\mathbf{A}_1 = \text{diag}(0, \Delta\varepsilon(\mathbf{r}), \dots, 0, 0), \quad (22)$$

while  $\mathbf{B}_1 = 0$ . We now determine the change in modal frequency for the cases when the metal in the metal-dielectric nanostructure is lossless and lossy.

### 5.1 Lossless case, $\Gamma_n = 0$

For the lossless case (12) both  $\mathbf{A}_0$  and  $\mathbf{B}_0$  are Hermitian. In this case, from (19), we have  $\mathbf{z}_0 = \mathbf{x}_0^\dagger$ . Thus, Eq. (20) reduces to

$$\omega_1 = -\omega_0 \frac{\mathbf{x}_0^\dagger \mathbf{A}_1 \mathbf{x}_0}{\mathbf{x}_0^\dagger \mathbf{A}_0 \mathbf{x}_0} = -\omega_0 \frac{\int d\mathbf{r} \Delta\varepsilon(\mathbf{r}) |\mathbf{E}(\mathbf{r})|^2}{\int d\mathbf{r} W_0}. \quad (23)$$

For the lossless dispersive system, we thus obtain a result that has the same form as (2) that is now appropriate for a system with dispersion, provided that we consider the total energy density in the system including contributions from the auxiliary mechanical fields. The expression for total energy, Eq. (11), has contributions from multiple Lorentz poles and is a multi-pole extension of the energy density expression previously derived by taking electric polarization into account explicitly [61,62]. For the lossless case this reduces to the usual expression for energy density in metals [61]

$$W_0 = \frac{1}{4} \left[ \frac{d(\omega\varepsilon\varepsilon_\infty)}{d\omega} \right] |\mathbf{E}|^2 + \frac{\mu_0}{4} |\mathbf{H}|^2. \quad (24)$$

## 5.2 Lossy case, $\Gamma_n \neq 0$

For the lossy case, the matrix  $\mathbf{B}_0$  in (16) is no longer Hermitian and  $\mathbf{z}_0 \neq \mathbf{x}_0^\dagger$ . Thus, Eq. (20) in this case reduces to

$$\omega_1 = -\omega_0 \frac{\mathbf{z}_0 \mathbf{A}_1 \mathbf{x}_0}{\mathbf{z}_0 \mathbf{A}_0 \mathbf{x}_0}. \quad (25)$$

While no explicit expression analogous to (2) can be written for the lossy case, Eq. (25) still allows one to calculate the frequency shift due to a dielectric refractive index change in the presence of a lossy metal; an important ability in realistic plasmonic sensing schemes.

Eq. (25) represents the technically correct way to do perturbation theory, where one needs to determine both the left and right eigenvectors of the general eigenvalue problem. Moreover the denominator in (25) cannot be interpreted as an energy integral. Empirically, on the other hand, we will show numerically that in fact  $\mathbf{z}_0 \approx \mathbf{x}_0^\dagger$ , even for metals with realistic loss parameters, and thus the denominator of (25),

$$\mathbf{z}_0 \mathbf{A}_0 \mathbf{x}_0 \approx \int d\mathbf{r} W_0, \quad (26)$$

where  $W_0$  is the energy density of the mode for the lossy system as defined in (11), which includes contributions from the mechanical auxiliary fields. We note that in a lossy system, when multiple poles are involved, there is no simple relation such as (24) that can be used to describe the total energy. Instead, the definition of (11), which explicitly takes into account contributions from the auxiliary mechanical fields, must be used.

## 5.3 Numerical example

Motivated by a recent experiment [20], we consider the model system introduced in Section 2. It consists of a two-dimensional periodic array of square plasmonic rods in air that are uniform along the third  $z$  direction. The system has periodicity  $a = 130\text{nm}$  and the rod has a side length of  $s = 0.45a = 58.5\text{ nm}$ .

To verify the accuracy of our perturbation theory approach we highlight a region of the TE band structure featuring both a surface and non-surface mode in Figure 3. We alter the dielectric constant of the dielectric region by  $\Delta\varepsilon = 0.02$ , and calculate the resulting shift in eigenfrequency, using perturbation theory for both lossy and lossless cases. For the lossless system, we set  $\Gamma_n = 0$ , and use (23). For the lossy system, we can use the exact perturbation theory result of (25), as well as the approximation in terms of energy density in (26). The results from these two forms of perturbation theory are nearly identical to each other. These results, from both forms of the perturbation theory, are then compared to the band structure obtained by directly solving (12) for the perturbed system. The results from the perturbation theory show excellent agreement with results from the direct calculation for both the lossless and lossy systems.

To illustrate the practical significance of this result, we analyze a refractive-index sensing scheme by calculating the reflection/transmission spectrum of 50-layers of the plasmonic rod system considered above, using a full-field 2D finite-difference frequency-domain (FDFD) simulation [36]. The plasmonic metal, corresponding as before to the two-pole fit of silver's dielectric function, is assumed to be lossless for the purposes of this illustration. For the TM case, below the cutoff frequency  $\omega_c$  (Figure 2(a)), no propagating modes are supported. Thus, the structure is strongly reflecting. The lowest-frequency dip in the reflection spectrum (Figure 4) corresponds to the first mode supported by the system, identified previously in Figure 2(a) at  $\omega_c$ . We can then examine the shift in this reflectivity dip when the dielectric surrounding the rods is changed by  $\Delta\varepsilon$  (due to, for example, the introduction of a biochemical analyte). We observe a shift of the dip by  $\Delta\omega = -9.9e - 5$  for  $\Delta\varepsilon = 1e - 3$ . Using (23) we calculate the shift of the lowest-frequency mode at  $k = 0$ , for the same  $\Delta\varepsilon$ , to be  $\omega_1 = -9.37e - 5$ , which matches well with the shift observed in the full-field simulation. Thus, the perturbation theory with respect to the eigenmodes of the system can be used to predict shifts in features of the same system's transmission and reflection spectra.

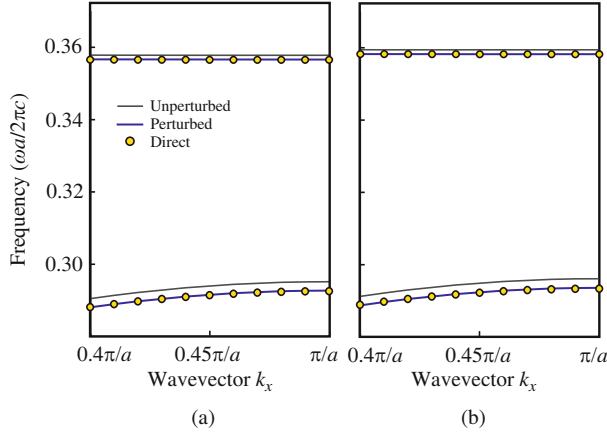


**Figure 3** Comparing the perturbation theory prediction (‘Perturbed’) and direct solution (‘Direct’) of  $\omega_1$  in the region identified in Figure 2(b), for dielectric  $\Delta\varepsilon(\mathbf{r}) = 0.02$ . The (a) lossless metal ( $\Gamma_n = 0$ ) and (b) lossy metal cases shows excellent agreement for both the flat surface mode and non-surface mode.

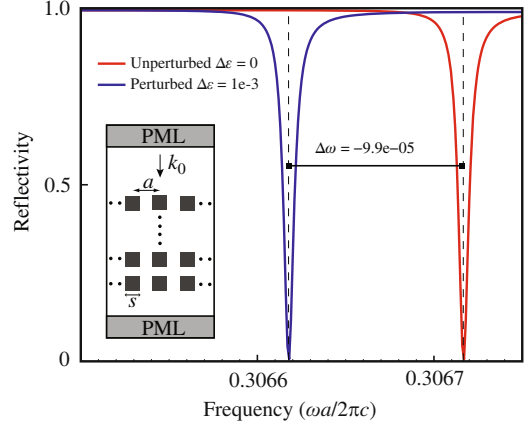


**Figure 4** Reflectivity spectrum of a finite 2D square lattice of square plasmonic rods ( $s = 0.45a$ ) in air, consisting of 50 layers. The results are obtained with a full-field FDFD simulation (shown in the inset schematic) and show a reflectivity dip corresponding to the lowest-frequency propagating mode in the system (the mode at  $\omega_c$  in Figure 2(a)). Altering the air region by  $\Delta\varepsilon = 1e-3$  to simulate a perturbation, a shift in the dip of  $\Delta\omega = -9.9e-5$  is observed, matching the theoretical prediction of (23),  $\omega_1 = -9.37e-5$ , well.

## 6 Upper bound on the modal material loss rate

In this section we review a fundamental analysis proving that, for any electromagnetic mode of a plasmonic metamaterial structure, there exists an upper bound on its material loss rate [41]. When the plasmonic material is described by a multi-pole Lorentz model, the upper bound is a frequency-dependent weighted-average of the damping rates of the oscillators that underlie the poles. We validate this proof by full-field simulations of a variety of systems including periodic arrays of slot antennas.

The past decade has seen many numerical studies of the loss properties of plasmonic and metamaterial structures [24,32,63–68]. The calculation of the modal material loss rate has also been used to understand the effect of plasmonic loss in solar cell light trapping schemes [69]. However, only a few recent papers have attempted to understand the general behavior of loss in plasmonic systems from a purely analytic perspective [70,71]. In contrast to these previous works, we review an analysis in this section that is not restricted to the quasi-static limit, any specific geometry or the Drude model. It is fully analytic and rigorous, derived directly from Maxwell’s equations and for material systems described by an arbitrary number of lossy Lorentz poles.

### 6.1 Derivation of the upper bound

To begin our analysis we first recast (2) by noting the Thomas-Reiche-Kuhn sum rule [72]  $\sum_{n=1}^N \omega_{p,n}^2 = n_e e^2 / m \varepsilon_\infty \equiv \omega_p^2$  where  $e$  and  $m$  are the charge and effective mass of electrons respectively. Using the rule, we can express the oscillator strength of each pole as  $\omega_{p,n}^2 = f_n \omega_p^2$  where  $\sum_{n=1}^N f_n = 1$ .

Solving the eigenvalue problem defined by (7)–(10) results in eigenfrequencies  $\omega = \omega_r + i\gamma$  that are complex in general, with  $\omega_r$  corresponding to the modal frequency and  $\gamma$  the mode’s material loss rate. Below we will use (7)–(10) to constrain the behavior of the modal material loss rate  $\gamma$ .

From (7)–(10) we obtain

$$(\omega_r + i\gamma) \left[ \mu_0 \mathbf{H}^* \cdot \mathbf{H} + \sum_{n=1}^N \frac{1}{f_n \omega_p^2 \varepsilon_\infty} \mathbf{V}_n^* \cdot \mathbf{V}_n \right] - \sum_{n=1}^N \frac{i\Gamma_n}{f_n \omega_p^2 \varepsilon_\infty} \mathbf{V}_n^* \cdot \mathbf{V}_n$$

$$= (\omega_r - i\gamma) \left[ \varepsilon_\infty \mathbf{E}^* \cdot \mathbf{E} + \sum_{n=1}^N \frac{\omega_{0,n}^2}{f_n \omega_p^2 \varepsilon_\infty} \mathbf{P}_n^* \cdot \mathbf{P}_n \right] + i(\mathbf{H}^* \cdot (\nabla \times \mathbf{E}) - \mathbf{E} \cdot (\nabla \times \mathbf{H}^*)). \quad (27)$$

We integrate both sides of (27) over space. We use the standard vector field identity on the last term of (27) and find a  $\int d\mathbf{r} \nabla \cdot (\mathbf{E} \times \mathbf{H}^*)$  term. For closed or periodic systems this term is zero, and in practice it is  $\approx 0$  for many open systems of interest where the field is strongly confined to a metal-dielectric interface. We then separate the real and imaginary components of (27) respectively to find the first result of this section

$$\int d\mathbf{r} \left( \mu_0 |\mathbf{H}|^2 + \sum_{n=1}^N \frac{1}{f_n \omega_p^2 \varepsilon_\infty} |\mathbf{V}_n|^2 \right) = \int d\mathbf{r} \left( \varepsilon_\infty |\mathbf{E}|^2 + \sum_{n=1}^N \frac{\omega_{0,n}^2}{f_n \omega_p^2 \varepsilon_\infty} |\mathbf{P}_n|^2 \right), \quad (28)$$

and

$$\gamma = \frac{\int d\mathbf{r} \sum_{n=1}^N (\Gamma_n / 4 f_n \omega_p^2 \varepsilon_\infty) |\mathbf{V}_n|^2}{\int d\mathbf{r} W_0}. \quad (29)$$

We emphasize that both (28) and (29) are exact for closed and periodic systems, and in practice accurately describe many open plasmonic systems of interest. Eq. (28) states that, for a given mode, the sum of the magnetic energy and kinetic energy of the electrons is equal to the sum of the electric energy and potential energy of the electrons. Eq. (29) relates the modal material loss rate to the fraction of its total energy that is in the kinetic energy of the electrons.

Comparing (11) and (28) directly leads to an exact bound on the kinetic energy of the electrons that is quantified by the  $\mathbf{V}$  field:

$$\int d\mathbf{r} \sum_{n=1}^N \frac{1}{4 f_n \omega_p^2 \varepsilon_\infty} |\mathbf{V}_n|^2 \leq \int d\mathbf{r} \frac{1}{2} W_0. \quad (30)$$

Substituting (30) into (29) we express the upper bound as

$$\gamma \leq \frac{1}{2} \frac{\sum_{n=1}^N \Gamma_n \int d\mathbf{r} \frac{1}{f_n \omega_p^2 \varepsilon_\infty} |\mathbf{V}_n|^2}{\sum_{n=1}^N \int d\mathbf{r} \frac{1}{f_n \omega_p^2 \varepsilon_\infty} |\mathbf{V}_n|^2} = \gamma_{\max}(\omega). \quad (31)$$

From (10) we find the following expression for  $|\mathbf{V}_n|^2$ :

$$\frac{1}{f_n \omega_p^2 \varepsilon_\infty} |\mathbf{V}_n|^2 = \frac{(\omega_r^2 + \gamma^2) f_n \omega_p^2 \varepsilon_\infty}{[\omega_{0,n}^2 - (\omega_r^2 + \gamma^2 + \gamma \Gamma_n)]^2 + (\omega_r \Gamma_n - 2\gamma \omega_r)^2} |\mathbf{E}|^2. \quad (32)$$

Substituting (32) into (31) we find a self-consistent expression for  $\gamma_{\max}$ :

$$\gamma \leq \frac{\sum_{n=1}^N \frac{\Gamma_n}{2} \frac{f_n}{[\omega_{0,n}^2 - (\omega_r^2 + \gamma^2 + \gamma \Gamma_n)]^2 + (\omega_r \Gamma_n - 2\gamma \omega_r)^2}}{\sum_{n=1}^N \frac{f_n}{[\omega_{0,n}^2 - (\omega_r^2 + \gamma^2 + \gamma \Gamma_n)]^2 + (\omega_r \Gamma_n - 2\gamma \omega_r)^2}} \equiv \gamma_{\max}(\omega_r). \quad (33)$$

However, in the optical and terahertz regimes relevant to plasmonics,  $\gamma \ll \omega_r$  and it is not necessary to solve this self-consistent equation. This allows us to eliminate the  $\gamma$  on the left hand side of the equation that makes it a self-consistent inequality and instead reduces to a simple bound:

$$\gamma_{\max}(\omega_r) = \frac{\sum_{n=1}^N \frac{\Gamma_n}{2} \frac{f_n}{(\omega_{0,n}^2 - \omega_r^2)^2 + \omega_r^2 \Gamma_n^2}}{\sum_{n=1}^N \frac{f_n}{(\omega_{0,n}^2 - \omega_r^2)^2 + \omega_r^2 \Gamma_n^2}}. \quad (34)$$

By defining weighting terms  $\theta_n(\omega_r)$

$$\theta_n(\omega_r) = \frac{f_n / ((\omega_{0,n}^2 - \omega_r^2)^2 + \omega_r^2 \Gamma_n^2)}{\sum_{n=1}^N f_n / ((\omega_{0,n}^2 - \omega_r^2)^2 + \omega_r^2 \Gamma_n^2)}, \quad (35)$$

we find the second result of this section

$$\gamma_{\max}(\omega_r) = \sum_{n=1}^N \theta_n(\omega_r) \frac{\Gamma_n}{2}, \quad (36)$$

where  $\sum_{n=1}^N \theta_n(\omega_r) = 1$ .

This expression is an approximation derived in the limit that  $\gamma \ll \omega_r$  which corresponds to most metamaterial situations of interest. The upper bound  $\gamma_{\max}(\omega_r)$  is a frequency-dependent weighted-average of one-half the damping rates of the poles,  $\Gamma_n/2$ . The weighting takes into account both the strength of the damping and the strength of the pole itself. Thus a weak pole (small  $f_n$ ) has limited effect on the upper bound even if it has an extremely large corresponding damping rate  $\Gamma_n$ . The behavior of the upper bound is thus complex and depends on the distributions of pole parameters for a material. As such, the maximum upper bound over all frequencies will not necessarily be  $\max(\Gamma_n)/2$  and, as we show in the numerical results, it can be substantially lower than this value.

To further examine the implications of these results we briefly review a few special cases that are of practical interest:

- 1) Single-pole case: The upper bound is exactly  $\gamma_{\max} = \Gamma_1/2$  for all frequencies.
- 2) Multi-pole case: Suppose there exists a  $k$ th pole with its frequency far away from other poles such that  $\theta_k(\omega_r) \gg \theta_n(\omega_r)$ ,  $n \neq k$ . Near this  $k$ th pole then we have  $\gamma_{\max} \simeq \frac{1}{2}\Gamma_k$ . This is particularly relevant when one has a Drude term as characterised by a resonant frequency  $\omega_0 = 0$  and a damping rate  $\Gamma_{\text{Drude}}$ . In such cases, the Drude damping rate dominates for low frequencies away from the lowest frequency Lorentz pole and  $\gamma_{\max} \simeq \Gamma_{\text{Drude}}/2$ .
- 3) High-frequency limit: The upper bound in this case is a constant sum of the damping rates of the oscillators weighted by the strength of each oscillator:

$$\gamma_{\max}(\omega_r \rightarrow \infty) = \sum_{n=1}^N f_n \Gamma_n. \quad (37)$$

The upper bound on  $\gamma$  corresponds to a lower bound on the intrinsic quality factor  $Q_i \geq \omega_r/2\gamma_{\max}(\omega_r)$ . These bounds are purely dependent on material properties and cannot be overcome by varying a plasmonic nanostructure's shape or design. Moreover, as we show in the numerical examples below, plasmonic modes with EM fields confined to deep subwavelength regions are often very close to this limit.

## 6.2 Numerical verification

We now numerically verify this result by calculating  $\gamma$  for the eigenmodes of a variety of plasmonic nanostructures either analytically or numerically using the method described in Section 2. First, we use a  $N = 1$  Drude fit of silver where  $\varepsilon_\infty = \varepsilon_0$ ,  $\omega_0 = 0$ ,  $\omega_p = 2\pi c/a$ , and  $\Gamma = 0.0025\omega_p$  for  $a = 136$  nm. We begin with a metal-air interface and calculate  $\gamma$  analytically for the fundamental surface plasmon mode. The modal loss rate of the fundamental surface plasmon mode of a Drude metal-air interface can be derived for steady-state analytically [41]. Using this analytical expression, we show in Figure 5 that  $\gamma$  indeed saturates at  $\gamma_{\max} = \Gamma/2$  as  $k_x \rightarrow \infty$ . For a metal-air interface this corresponds to  $\omega_r \rightarrow \omega_p/\sqrt{2} \equiv \omega_{\text{sp}}$ , the surface plasmon frequency.

Next we consider a more complex plasmonic nanostructure consisting of a 2D periodic array of silver slot antennas in air. For the plasmonic material we use a  $N = 3$  fit of silver [41]. We plot the corresponding  $\gamma_{\max}(\omega_r)$  in Figure 6(a). In consistency with case (2) of the theory presented earlier, we observe that in the frequency region near a pole  $\gamma_{\max}(\omega_r)$  is dominated by the damping rate of such a pole. In frequency regions between poles,  $\gamma_{\max}(\omega_r)$  is a weighted average of the damping rates of the poles. Furthermore, in this example the maximum of the upper bound is in fact lower than the largest damping rate,  $\Gamma_3/2$ , due to the complex interaction of the strengths and damping terms of these three Lorentz poles.

Having discussed the upper bound of the modal material loss rate, which is determined by the plasmonic material model only, we now consider the material loss rate of the optical modes of the antenna array. We calculate  $\gamma$  of TE ( $E_x$  and  $E_y$  in-plane) modes for all wave vectors  $k$  in the irreducible first Brillouin

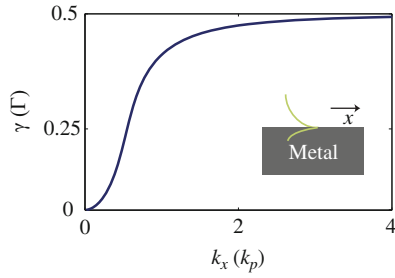


**Figure 5** Modal material loss rate ( $\gamma$  in units of  $\Gamma$ ) vs. wave vector ( $k_x$  in units of  $k_p$ ) for a planar metal-air interface calculated analytically. The metal is described by  $\varepsilon(\omega) = 1 - \omega_p^2/(\omega - i\Gamma)$ , and  $k_p = \omega_p/c$ .  $\gamma$  approaches  $\gamma_{\max} = \Gamma/2$  for large  $k_x$ , where the field is strongly confined spatially to the interface. Figure from [41].

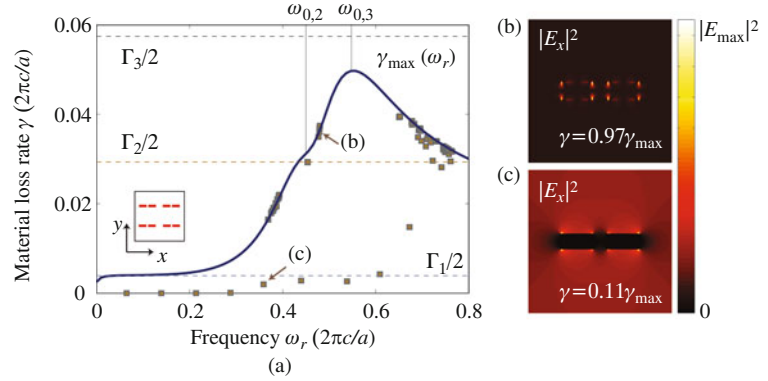


**Figure 6** (a) Modal material loss rate ( $\gamma$  in units of  $2\pi c/a$ , where  $a = 136$  nm is the period) vs. real frequency ( $\omega_r$  in units of  $2\pi c/a$ ) for all TE modes of a 2D periodic array of plasmonic slot antennas (shown in the inset) in the first Brillouin zone. The plasmonic material is described by a three-pole fit of silver's dielectric function [41]. The  $\gamma$  values, numerically calculated via the method of Section 2, are shown as individual points. Many modes follow the upper bound  $\gamma_{\max}$  (marked by the blue line) but do not exceed it. (b),(c) Electric field intensity ( $|E_x|^2$ ) of two eigenmodes with large and small  $\gamma$ . The modes with larger  $\gamma$  that approach  $\gamma_{\max}$  exhibit field profiles that are strongly concentrated along the metal-air interfaces of the antenna. Figure from [41].

zone. These  $\gamma$  are plotted against their corresponding real frequency  $\omega_r$  in Figure 6(a) as squares. As in Figure 5 the numerically calculated  $\gamma$  for the antenna array's optical modes do not exceed the predicted upper bound of  $\gamma_{\max}(\omega_r)$ , but many modes do approach this bound. We compare two modes with large and small  $\gamma$  in Figure 6(b) and Figure 6(c) respectively. The eigenmode with strong field confinement (Figure 6(b)) at the metal-air interface has a large  $\gamma$ , approaching the limit of  $\gamma_{\max}$ .

As an added example we numerically calculate the material loss rate of a 2D periodic array of air holes in silver. We plot the corresponding  $\gamma_{\max}(\omega_r)$  in, and show the cavity array schematically in the inset of, Figure 7. As in Figure 6(a) we plot the upper bound  $\gamma_{\max}(\omega_r)$  and again observe that  $\gamma_{\max}(\omega_r)$  is dominated by the damping rates of poles in frequency regions surrounding them, but otherwise is a weighted average in frequency regions between poles. As in Figure 5  $\gamma$  does not exceed the predicted  $\gamma_{\max}(\omega_r)$ , but many modes do approach the limit. Through these numerical examples, we have demonstrated that the upper bound as derived theoretically can indeed be used to constrain modal loss behavior in plasmonic structures in a general multi-pole, multiple mode situation.

## 7 Conclusion

In this review, we first discussed a metamaterial band theory that rigorously models the behavior of plasmonic nanostructures and metamaterials over a broad range of frequencies [39]. The specific approach used couples the mechanical motion of electrons in the metals to Maxwell's equations as a linear system and formulates the band structure calculation as a standard eigenvalue equation. In the lossless case the equation is Hermitian and the eigenmodes form a complete orthonormal basis. We numerically demonstrated the efficacy of this approach by computing the band structure of 2D periodic systems. More recently, other researchers have extended this to 3D and used this formalism to compute the photonic band structure of 3D periodic metamaterial systems [3]. Indeed, there is substantial demand in the metamaterial community for the ability to compute the band structure of 3D systems numerically.

We next used the band theory to develop a metamaterial perturbation theory that rigorously treats the effect of small variations and changes in plasmonic nanostructures and metamaterials [40]. We considered an example of such a variation: the dielectric refractive-index in a metal-dielectric system. While this example is of both fundamental and applied interest, we emphasize that the perturbation

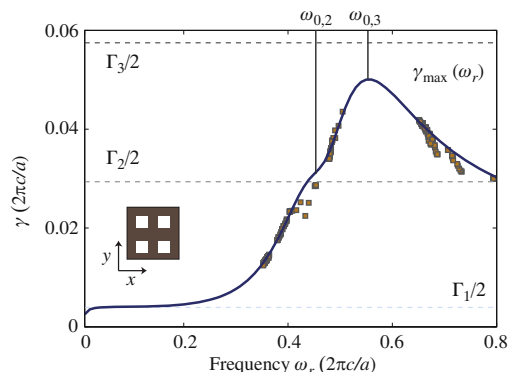


**Figure 7** Material loss rate ( $\gamma$  in units of  $2\pi c/a$ , where  $a = 136$  nm is the period) vs. real frequency ( $\omega_r$  in units of  $2\pi c/a$ ) for TE modes of a 2D periodic array of air holes in a plasmonic material (shown in the inset) in the first Brillouin zone. The plasmonic material is described by a three-pole fit of silver's dielectric function [41]. The  $\gamma$  values, numerically calculated via the method of Section 2, are plotted as squares. Many modes follow the upper bound  $\gamma_{\max}$  (marked by the blue line) but do not exceed it. Note here that as in Figure 6(a)  $\gamma_{\max}$  is frequency-dependent because of the presence of multiple poles and that its value, and the loss rates of the system's modes, are influenced by the damping rate of the pole closest to the mode's real frequency but are substantially below the largest damping rate. Figure from [41].

theory itself is very general. Two recent works have used our approach to treat the effect of nonlinearities [73] and coupling between resonators [74] in plasmonic and metamaterial systems. In addition, we see opportunities to understand the effect of fabrication imperfections and other geometric variations using the perturbation theory presented in this paper.

Optical loss in metallic nanostructures has been a topic of great concern and research interest from the earliest days of metamaterials research. We have reviewed an analytical derivation of an exact energy relation between the electromagnetic fields and the mechanical motion of electrons in dispersive plasmonic and metamaterial systems [41]. We then showed how this relation places an upper bound on the material loss rate of optical modes in such dispersive systems, and verified this result numerically. We highlight here again that these results were derived exactly without electrostatic approximations and apply generally to electromagnetic modes in any dispersive material system, including polaritonic materials. This analytical framework and bound together place strong constraints on using metamaterial approaches to maximize broadband absorption for photodetection and solar applications, topics of very recent interest that have attracted much attention from the broader research community.

As research in metamaterials and nanophotonics expands to a broader range of fundamental and applied topics, we anticipate the band theory and related extensions presented herein will prove an elucidative framework for future inquiry.

## Acknowledgements

This work was supported by AFOSR MURI Programs FA9550-12-1-0471 and FA9550-09-1-0704, and by U.S. Department of Energy (Grant No. DE-FG02-07ER46426).

## References

- 1 Chen X D, Grzegorzczak T M, Wu B I, et al. Robust method to retrieve the constitutive effective parameters of metamaterials. *Phys Rev E*, 2004, 70: 016608
- 2 Valentine J, Zhang S, Zentgraf T, et al. Three-dimensional optical metamaterial with a negative refractive index. *Nature*, 2008, 455: 376–379
- 3 Hur K, Francescato Y, Giannini V, et al. Three-dimensionally isotropic negative refractive index materials from block copolymer self-assembled chiral gyroid networks. *Angew Chem Int Ed*, 2011, 50: 11985–11989
- 4 Joannopoulos J D, Johnson S G, Winn J N, et al. *Photonic Crystals: Molding the Flow of Light*. 2nd ed. Princeton: Princeton University Press, 2008
- 5 Johnson S, Joannopoulos J. Block-iterative frequency-domain methods for Maxwell's equations in a planewave basis. *Opt Express*, 2001, 8: 173–190

- 6 Busch K, Mingaleev S F, Garcia-Martin A, et al. The wannier function approach to photonic crystal circuits. *J Phys-Condens Matter*, 2003, 15: R1233–R1256
- 7 Jiao Y, Fan S H, Miller D A B. Systematic photonic crystal device design: global and local optimization and sensitivity analysis. *IEEE J Quantum Electron*, 2006, 42: 266–279
- 8 Kuzmiak V, Maradudin A A, McGurn A R. Photonic band structures of two-dimensional systems fabricated from rods of a cubic polar crystal. *Phys Rev B*, 1997, 55: 4298–4311
- 9 Kuzmiak V, Maradudin A A. Photonic band structures of one- and two-dimensional periodic systems with metallic components in the presence of dissipation. *Phys Rev B*, 1997, 55: 7427–7444
- 10 Kuzmiak V, Maradudin A A. Distribution of electromagnetic field and group velocities in two-dimensional periodic systems with dissipative metallic components. *Phys Rev B*, 1998, 58: 7230–7251
- 11 Pendry J B. Calculating photonic band structure. *J Phys-Condens Matter*, 1996, 8: 1085–1108
- 12 Sakoda K, Kawai N, Ito T, et al. Photonic bands of metallic systems. i. principle of calculation and accuracy. *Phys Rev B*, 2001, 64: 045116
- 13 Huang K C, Bienstman P, Joannopoulos J D, et al. Field expulsion and reconfiguration in polaritonic photonic crystals. *Phys Rev Lett*, 2003, 90: 196402
- 14 Ito T, Sakoda K. Photonic bands of metallic systems. 5. features of surface plasmon polaritons. *Phys Rev B*, 2001, 64: 045117
- 15 Toader O, John S. Photonic band gap enhancement in frequency-dependent dielectrics. *Phys Rev E*, 2004, 70: 046605
- 16 Moreno E, Erni D, Hafner C. Band structure computations of metallic photonic crystals with the multiple multipole method. *Phys Rev B*, 2002, 65: 155120
- 17 McPhedran R C, Botten L C, McOrist J, et al. Density of states functions for photonic crystals. *Phys Rev E*, 2004, 69: 016609
- 18 Homola J. Present and future of surface plasmon resonance biosensors. *Anal Bioanal Chem*, 2003, 377: 528–539
- 19 Homola J, ed. *Surface Plasmon Resonance Based Sensors*. Berlin: Springer, 2006
- 20 Kabashin A, Evans P, Pastkovsky S. Plasmonic nanorod metamaterials for biosensing. *Nat Mat*, 2009, 8: 867–871
- 21 Rosenberg J, Shenoi R V, Vandervelde T E, et al. A multispectral and polarization-selective surface-plasmon resonant midinfrared detector. *Appl Phys Lett*, 2010, 95: 161101
- 22 Alleyne C, Kirk A, McPhedran R. Enhanced spr sensitivity using periodic metallic structures. *Opt Express*, 2007, 15: 8163–8169
- 23 Dionne J A, Diest K, Sweatlock L A, et al. Plasmostor: a metal-Oxide-Si field effect plasmonic modulator. *Nano Lett*, 2009, 9: 897–902
- 24 Cai W S, White J S, Brongersma M L. Compact, high-speed and power-efficient electrooptic plasmonic modulators. *Nano Lett*, 2009, 9: 4403–4411
- 25 Fan S H. Nanophotonics: magnet-controlled plasmons. *Nat Photon*, 2010, 4: 76–77
- 26 Pala R A, Shimizu K T, Melosh N A, et al. A nonvolatile plasmonic switch employing photochromic molecules. *Nano Lett*, 2008, 8: 1506–1510
- 27 Pacifici D, Lezec H J, Atwater H A. All-optical modulation by plasmonic excitation of cdse quantum dots. *Nat Photon*, 2007, 1: 402–406
- 28 Ozbay E. Plasmonics: merging photonics and electronics at nanoscale dimensions. *Science*, 2006, 311: 189–193
- 29 Atwater H A, Polman A. Plasmonics for improved photovoltaic devices. *Nat Mat*, 2010, 9: 205–213
- 30 Boltasseva A, Atwater H A. Low-loss plasmonic metamaterials. *Science*, 2011, 331: 290–291
- 31 Sorger V J, Oulton R F, Yao J, et al. Plasmonic fabry-pérot nanocavity. *Nano Lett*, 2009, 9: 3489–3493
- 32 Halas N J, Lal S, Chang W S, et al. Plasmons in strongly coupled metallic nanostructures. *Chem Rev*, 2011, 111: 3913–3961
- 33 Ruan Z C, Yan M, Neff C W, et al. Ideal cylindrical cloak: perfect but sensitive to tiny perturbations. *Phys Rev Lett*, 2007, 99: 113903
- 34 Novotny L. Effective wavelength scaling for optical antennas. *Phys Rev Lett*, 2007, 98: 266802
- 35 Brongersma M L. Plasmonics: engineering optical nanoantennas. *Nat Photon*, 2008, 2: 270–272
- 36 Veronis G, Dutton R W, Fan S H. Metallic photonic crystals with strong broadband absorption at optical frequencies over wide angular range. *J Appl Phys*, 2005, 97: 093104
- 37 Aydin K, Ferry V E, Briggs R M, et al. Broadband polarization-independent resonant light absorption using ultrathin plasmonic super absorbers. *Nat Commun*, 2011, 2: 517
- 38 Knight M W, Sobhani H, Nordlander P, et al. Photodetection with active optical antennas. *Science*, 2011, 332: 702–704
- 39 Raman A, Fan S H. Photonic band structure of dispersive metamaterials formulated as a hermitian eigenvalue problem. *Phys Rev Lett*, 2010, 104: 087401
- 40 Raman A, Fan S H. Perturbation theory for plasmonic modulation and sensing. *Phys Rev B*, 2011, 83: 205131
- 41 Raman A, Shin W, Fan S H. Upper bound on the modal material loss rate in plasmonic and metamaterial systems.

- Phys Rev Lett, 2013, 110: 183901
- 42 Drachev V P, Chettiar U K, Kildishev A V, et al. The ag dielectric function in plasmonic metamaterials. *Opt Express*, 2008, 16: 1186–1195
  - 43 Taflove A, Hagness S C. *Computational Electrodynamics: the Finite-Difference Time-Domain Method*. 3rd ed. Artech House Publishers, 2005
  - 44 Joseph R M, Hagness S C, Taflove A. Direct time integration of Maxwell's equations in linear dispersive media with absorption for scattering and propagation of femtosecond electromagnetic pulses. *Opt Lett*, 1991, 16: 1412–1414
  - 45 Bhat N A R, Sipe J E. Hamiltonian treatment of the electromagnetic field in dispersive and absorptive structured media. *Phys Rev A*, 2006, 73: 063808
  - 46 Yee K. Numerical solution of initial boundary value problems involving Maxwell's equations in isotropic media. *IEEE Trans Antennas Propag*, 1966, 14: 302–307
  - 47 Chen Y C, Sun K Q, Beker B, et al. Unified matrix presentation of Maxwell's and wave equations using generalized differential matrix operators [em engineering education]. *IEEE Trans Educ*, 1998, 41: 61–69
  - 48 Lehoucq R B, Sorensen D C, Yang C. *Arpack Users Guide: Solution of Large Scale Eigenvalue Problems by Implicitly Restarted Arnoldi Methods*. Society for Industrial & Applied, 1997
  - 49 Johnson P B, Christy R W. Optical constants of the noble metals. *Phys Rev B*, 1972, 6: 4370–4379
  - 50 Fan S H, Villeneuve P R, Joannopoulos J D. Large omnidirectional band gaps in metallodielectric photonic crystals. *Phys Rev B*, 1996, 54: 11245–11251
  - 51 Huang K C, Bienstman P, Joannopoulos J D, et al. Field expulsion and reconfiguration in polaritonic photonic crystals. *Phys Rev Lett*, 2003, 90: 196402
  - 52 Chow E, Grot A, Mirkarimi L W, et al. Ultracompact biochemical sensor built with two-dimensional photoniccrystal microcavity. *Opt Lett*, 2004, 29: 1093–1095
  - 53 Mortensen N, Xiao S, Pedersen J. Liquid-infiltrated photonic crystals—enhanced light-matter interactions for lab-on-a-chip applications. *Microfluid Nanofluid*, 2008, 4: 117
  - 54 White I, Fan X. On the performance quantification of resonant refractive index sensors. *Opt Express*, 2008, 16: 1020–1028
  - 55 Robinson J, Chen L, Lipson M. On-chip gas detection in silicon optical microcavities. *Opt Express*, 2008, 16: 4296–4301
  - 56 Dell'Olio F, Passaro V. Optical sensing by optimized silicon slot waveguides. *Opt Express*, 2007, 15: 4977–4993
  - 57 Joannopoulos J D, Johnson S G, Winn J N, et al. *Photonic Crystals: Molding the Flow of Light*. 2nd ed. Princeton: Princeton University Press, 2008
  - 58 Shao L H, Ruther M, Linden S, et al. Electromodulation of photonic metamaterials. In: *Photonic Metamaterials and Plasmonics*. Optical Society of America, 2010. MMC2
  - 59 Diest K. Active metal-insulator-metal plasmonic devices. Dissertation of Doctoral Degree. California: California Institute of Technology, 2010
  - 60 Guler U, Turan R. Effect of particle properties and light polarization on the plasmonic resonances in metallic nanoparticles. *Opt Express*, 2010, 18: 17322–17338
  - 61 Loudon R. The propagation of electromagnetic energy through an absorbing dielectric. *J Physics A-Gen Phys*, 1970, 3: 233–245
  - 62 Ruppin R. Electromagnetic energy density in a dispersive and absorptive material. *Phys Lett A*, 2002, 299: 309–312
  - 63 Zhang S, Fan W J, Malloy K J, et al. Near-infrared double negative metamaterials. *Opt Express*, 2005, 13: 4922–4930
  - 64 Dolling G, Wegener M, Soukoulis C M, et al. Design-related losses of double-fishnet negative-index photonic metamaterials. *Opt Express*, 2007, 15: 11536–11541
  - 65 Oulton R F, Bartal G, Pile D F P, et al. Confinement and propagation characteristics of subwavelength plasmonic modes. *New J Phys*, 2008, 10: 105018
  - 66 Khurgin J B, Sun G. In search of the elusive lossless metal. *Appl Phys Lett*, 2010, 96: 181102
  - 67 Ferry V E, Munday J N, Atwater H A. Design considerations for plasmonic photovoltaics. *Adv Mat*, 2010, 22: 4794–4808
  - 68 Shin W, Fan S H. Choice of the perfectly matched layer boundary condition for frequency-domain Maxwell's equations solvers. *J Comput Phys*, 2012, 231: 3406–3431
  - 69 Schiff E A. Thermodynamic limit to photonic-plasmonic light-trapping in thin films on metals. *J Appl Phys*, 2012, 110: 104501
  - 70 Wang F, Shen Y R. General properties of local plasmons in metal nanostructures. *Phys Rev Lett*, 2006, 97: 206806
  - 71 Khurgin J B, Sun G. Scaling of losses with size and wavelength in nanoplasmonics and metamaterials. *Appl Phys Lett*, 2011, 99: 211106
  - 72 Bethe H A, Salpeter E E. *Quantum Mechanics of One- and Two-Electron Atoms*. Berlin: Springer-Verlag, 1957
  - 73 Zeng Y, Dalvit D A R, O'Hara J, et al. Modal analysis method to describe weak nonlinear effects in metamaterials. *Phys Rev B*, 2012, 85: 125107
  - 74 Xi B, Xu H, Xiao S Y, et al. Theory of coupling in dispersive photonic systems. *Phys Rev B*, 2011, 83: 165115